Journal of Alloys and Compounds 481 (2009) 819–825

Contents lists available at ScienceDirect

Journal of Alloys and Compounds

journal homepage: www.elsevier.com/locate/jallcom

Influence of Ag, Cu dopants on the second and third harmonic response of ZnO films

B. Kulyk[a,c,*], B. Sahraoui[a], V. Figà[b], B. Turko[c], V. Rudyk[c], V. Kapustianyk[c]

[a] POMA Laboratory, FRE CNRS 2988 UFR Sciences, University of Angers, 2 Boulevard Lavoisier, 49045 Angers Cedex 01, France
[b] Department of Chemical, Process and Materials Engineering, University of Palermo, Viale delle Scienze, 90128 Palermo, Italy
[c] Scientific-Technical and Educational Center of Low Temperature Studies, Chair of Solid State Physics, Ivan Franko National University of Lviv, Dragomanova Street, 50, UA-79005 Lviv, Ukraine

ARTICLE INFO

Article history:
Received 15 January 2009
Received in revised form 15 March 2009
Accepted 20 March 2009
Available online 31 March 2009

Keywords:
Silver-doped ZnO film
Copper-doped ZnO film
RF-magnetron sputtering
SHG
THG

ABSTRACT

Silver- and copper-doped ZnO films were prepared by radio-frequency (RF)-magnetron sputtering on glass and quartz substrates. The influence of dopants content on the microstructural evolution and optical as well as nonlinear optical (NLO) properties were investigated. It has been found that the grain sizes were enlarged with increasing of Ag, Cu dopants amount in ZnO films. The Ag or Cu doping leads to the optical band gap narrowing. Besides, the second-order NLO response of Ag- and Cu-doped ZnO films is lower than that of undoped ZnO film. The second harmonic generation (SHG) efficiency of the ZnO:Ag film was found to be higher than that of the ZnO:Cu film at the similar concentration of dopant. In addition, the decrease of the third harmonic generation (THG) response is observed in ZnO films with increasing of Ag or Cu dopant amount.

1. Introduction

ZnO is a very interesting material for many different applications in both microelectronic and optoelectronic devices. It is a wide-band gap oxide semiconductor with a direct energy gap of about 3.37 eV and high exciton binding energy of 60 meV. Though, ZnO absorbs ultraviolet (UV) radiation due to band-to-band transition, it can be used as transparent conductive oxide thin film, mainly for applications such as solar cells, liquid crystal displays and heat mirrors [1–3]. Furthermore, ZnO is used as semiconducting multilayers, gas sensors and optical position sensors, UV light emitters, surface acoustic wave devices and piezoelectric transducers [4,5]. In the last few years, ZnO has emerged as one of the most promising materials due to its optical and electrical properties, high mechanical and chemical stability, together with its abundance in nature and nontoxicity. In order to improve the properties of ZnO films, several techniques such as sputtering [6–10], thermal evaporation [11], metal-organic chemical vapour deposition [12,13], spray pyrolysis [14] and pulsed laser deposition [15–17] have been applied for their production. Radio-frequency (RF) magnetron sputtering technique is one of preferred among these techniques since it is versatile and permits to produce the high-quality films for different applications.

The structural, physical and electrical properties of ZnO films were governed by deposition parameters [14], posttreatment [7,17,18] and doping material [6,15,12,19–22] such as Al, Ga, Sc, Y, Mn, Cu, Ag, etc. In addition, it is known that the metals of group I (Ag and Cu) are fast-diffusing impurities in the semiconductor compound [14]. The diffusion of copper or silver into ZnO can cause changes in the characteristics of its structure and, therefore, in the other physical properties.

The Ag and Cu dopants in ZnO may behave like many other monovalent dopant ions, which have the ability to occupy both the lattice and interstitial sites (i.e. amphoteric dopants), expressed as [19]:

$$2Ag \xrightarrow{ZnO} Ag_{Zn} + Ag_i \quad (1)$$

$$2Cu \xrightarrow{ZnO} Cu_{Zn} + Cu_i \quad (2)$$

The Ag and Cu centers in ZnO can occur in the following different charge states: Ag^0, Ag^+, Ag^{2+} [15] and Cu^0, Cu^+, Cu^{2+} [23], respectively. When Ag^+ or Cu^+ substitute Zn^{2+} they act as acceptor in ZnO, while the interstitial Ag^{2+} or Cu^{2+} are donors. However, Ag^0 and Ag^{2+} or Cu^0 and Cu^{2+} ions can easily lose or gain electron resulting in the formation of Ag^+ or Cu^+ that implies more centers, which are acceptors [15]. Beside these dopant centers, the other defects such as Zn_i, V_O, O_i and V_{Zn} can be created which occur even in undoped ZnO [7]. The Ag-, Cu-doped ZnO films taken in various concentrations were already studied by photosensitivity, lumines-

* Corresponding author. Tel.: +380509128436.
E-mail address: bohdan_kulyk@yahoo.com (B. Kulyk).

0925-8388/$ – see front matter © 2009 Elsevier B.V. All rights reserved.
doi:10.1016/j.jallcom.2009.03.117

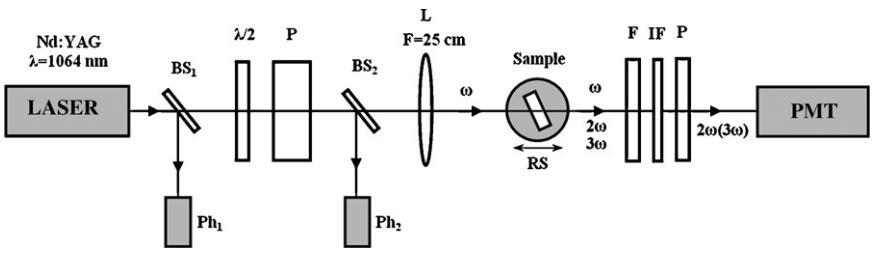

Fig. 1. Experimental setup for second harmonic generation (SHG) measurements: (BS_1 and BS_2) the beam splitters, (Ph_1 and Ph_2) the photodiodes, ($\lambda/2$) the half wave plate, (P) the Glan polarizer, (L) the lens, (RS) the rotation stage, (F) the filter/s, (IF) the interference filter and (PMT) the photomultiplier tube.

cent properties, electrical stability and have been used for different applications. However, there are not many reports on the study of nonlinear optical (NLO) properties of these films. Moreover, the Cu-doped ZnO films would be very interesting object for investigations of the photoinduced nonlinear optics phenomena, first of all, photoinduced second harmonic generation (SHG). Inducing a media by polarized external field (polarized laser field) can create a local photoinduced electric field inside giving additional increase to SHG even in metallic nanoparticles [24].

Coherent NLO phenomena such as SHG and third harmonic generation (THG) depends explicitly on the crystal lattice structure of the medium, which could yield to a very high polarization selectivity. Moreover, nonresonant SHG is essentially independent of wavelength below the energy band gap of semiconductor materials, most often including wavelength region typically used in optical fiber communications. Hence, characterizing the NLO response is crucial for evaluating potential applications [25].

In this paper, therefore, we investigated the effect of dopants on microstructural evolution, optical and NLO properties such as SHG and THG of Ag- and Cu-doped ZnO thin films. This work is a continuation of our previous work connected with NLO properties in ZnO structures [11,26-28].

2. Experimental details

The ZnO:Ag and ZnO:Cu thin films were deposited on glass and quartz substrates by means of RF-magnetron sputtering system using ZnO-powder targets together with metallic Ag or Cu in argon atmosphere at the gas pressure of 10^{-3} Torr. In order to minimize the thermal stresses, the substrate temperature was fixed at 300 °C. The target-to-substrate distance was 60 mm and RF-power –100 W.

The thickness of ZnO thin films was estimated by the deposition time and by Dektak surface stylus profiler (model Veeco) to be from 600 to 1200 nm. Scanning electron microscopy (SEM) images were recorded on a REMMA-102-02 scanning electron microscope, working at 20 kV dc acceleration voltages in vacuum. The atomic amount of Ag and Cu dopants in ZnO films [taken from energy-dispersive X-ray (EDX) analysis] was 1.6%, 5.9% and 4.7%, 71%, respectively. The atomic force microscopy (AFM) scans were performed in contact mode using the CP Research Thermomicroscope (Veeco). Processing of images was done using the WSxM4.0 program (Nanotec Electronica S. L.). The optical absorption spectra in visible and near UV region were measured using a Lambda 19 spectrometer from PerkinElmer.

The SHG as well as the THG measurements were carried out by means of the rotational Maker-fringe technique [29] in the transmission scheme (Fig. 1) for the s–p and p–p SHG polarization geometry of experiment. A crystalline *y*-cut quartz plate has been used as a reference material for SHG and fused silica plate for THG measurements.

As a fundamental beam, we used the output beam of a Q-switched Nd-doped yttrium–aluminum–garnet laser (model: Quantum Elite) generating at $\lambda = 1064$ nm with 16 ps pulse duration and 10 Hz repetition rate. The incident polarization was selected with a half-wave plate and polarizer in front of the focussing lens. The intensity at the input face of the sample is assumed to be a Gaussian distribution in space and time. The beam diameter was 0.4 mm at the film and the applied power density was in the range of 1–10 GW/cm^2. The beam was focused onto the sample with lens of 250 mm focal length. A motorized rotation stage with the mounted sample allowed the variation of the incident angle with a resolution of 1.0°. The interference filter (at 532 nm for SHG or at 355 nm for THG) was used to cut the pump beam before the photomultiplier. Detector saturation was prevented using linear neutral density filters, whose transmittance value was taken into account during data fitting. The polarization of the SHG or THG was checked with a polarizer placed behind the photomultiplier. The second and third harmonic signals were detected by the photomultiplier tube (model Hamamatsu), which was connected to a boxcar and processed by a computer. A portion of the input beam was selected and measured by a fast photodiode Ph_2 to monitor the input energy. Finally, we obtained the so-called Maker-fringes, which were generated by rotating the sample through the range of ±70° to the normal.

3. Results and discussion

3.1. Microstructure and morphology analysis

SEM and AFM micrograph analyses (Fig. 2) indicate the granular character of the deposited films. The average grain size and the surface roughness obtained from those micrographs are related to the amount of Ag and Cu dopants (Table 1). Typical grain size distribution curves for the Ag- and Cu-doped ZnO films are shown in Fig. 3. It is evident from Figs. 2 and 3 that a low amount of Ag or Cu (1.6 and 4.7 at.%) promotes the ZnO grain growth (Table 1). A larger amount of Ag (e.g. 5.9 at.%) induces appearance of larger grains and their average height increases together with surface roughness. The mean size of ZnO grains is strongly dependent on the amount of dopant. However, ZnO grains become dispersive with doping but it is evident from Fig. 3 that at the quite close amount of dopant (e.g. 5.9 and 4.7 at.%) the larger sizes of ZnO grains are observed in Cu-doped ZnO film. Such a difference in surface morphology of Ag- and Cu-doped ZnO films can be explained by the difference in mechanisms of dopant incorporation into ZnO structure.

As it is evident from previous reports, the Ag-doped ZnO films have preferred orientation in the (0 0 2) direction [6,7,9,13,15,19,30]. Because Ag^+ ions have larger radius (0.122 nm) than Zn^{2+} (0.074 nm), they either substitute ions of Zn^{2+} leading to the distortion of unit cell or segregate at the grain boundaries of ZnO and hence induce considerable disorder and faster grow of ZnO grains [19,30]. Ag^+ would preferentially choose to sit in the vicinity of grain boundaries due to its large ionic radius.

Similarly to this, the Cu-doped ZnO films show orientation in the (0 0 2) direction [8,10,13,14,16,17] and most Cu atoms occur as interstitial in the lattice of ZnO crystallites. The radius of Cu^{2+} (0.072 nm) is a little bit less, meanwhile, the radius of Cu^+ is larger than that of Zn^{2+} (0.074 nm). The substitution of Zn^{2+} ions is advantageous for Cu^{2+} because of their close radii. When Cu^{2+}ions substitute Zn^{2+} ions, the lattice constant decrease [10]. Besides, due to a small radius the copper ions can be interstitial dopants or would create the metallic clusters [23].

Table 1
Characteristics of ZnO films, undoped and doped by Ag and Cu.

Film	Roughness (nm)	Average height (nm)	Band gap energy (eV)
ZnO	3.2	14.1	3.29
ZnO:Ag(1.6 at.%)	22.6	70.9	3.26
ZnO:Ag(5.9 at.%)	35.6	102	3.07
ZnO:Cu(4.7 at.%)	22.1	116	3.23
ZnO:Cu(71 at.%)	–	–	2.15

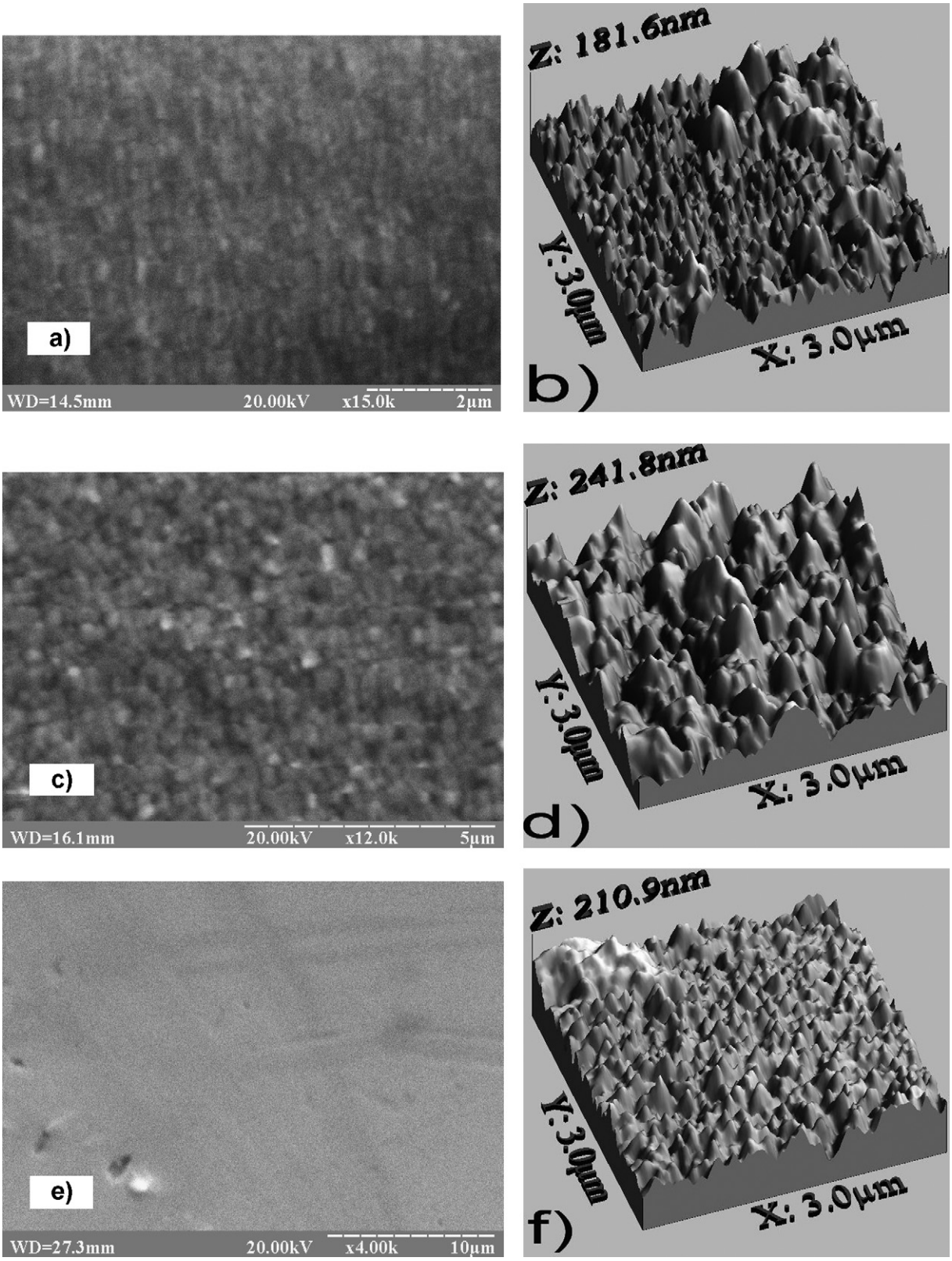

Fig. 2. SEM (left) and AFM (right) images of the (a and b) 1.6 at.% ZnO:Ag, (c and d) 5.9 at.% ZnO:Ag and (e and f) 4.7 at.% ZnO:Cu.

3.2. Optical absorption measurements

We measured the optical absorption spectra in the visible and near UV for ZnO films with different Ag, Cu concentrations (Fig. 4a. The optical band gap (E_g) of the Ag- and Cu-doped ZnO films can be obtained by plotting $(\alpha h\nu)^2$ vs. $h\nu$ (α is absorption coefficient and $h\nu$ is photon energy) and extrapolating the straight-line portion of this plot to the photon energy axis. Fig. 4b shows the variation of the optical band gap as a function of Ag and Cu content, respectively. It is demonstrated that the band gap is narrowing with increasing

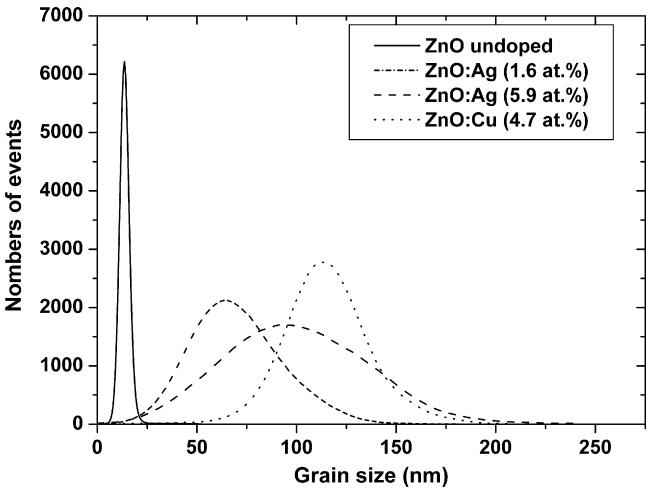

Fig. 3. Grain size distributions of undoped, 1.6 and 5.9 at.% Ag-doped and 4.7 at.% Cu-doped ZnO samples.

dopants content. The main reason is that the Zn^{2+} ions are substituted by the Ag^{+} or Cu^{2+} ions. The substitution by the Cu^{2+} ions of less radius than that of the Zn^{2+} leads to the decrease of optical band gap rather than by larger Ag^{+} ions at the similar amount of dopant (Table 1). These results are in good agreement with that obtained by Jeong et al. [6] for Ag-doped ZnO films. In the highly doped by copper (about 71 at.%) ZnO film the band gap energy is close to that of Cu_2O phase which is equal to 2.1 eV [31]. In addition, the decrease of the transmission of ZnO by doping with Ag, Cu can be explained by the influence of near-band levels, arising due to the introduction of dopant.)

Obtained spectra show that the samples do not absorb at the wavelength of laser excitation (1064 nm), therefore, we do not deal with the resonant effects during high harmonic generation processes.

3.3. SHG measurements

The SHG measurements were performed by rotational Maker fringe technique for s- and p-polarized fundamental beam. Taking into account that the structure of ZnO belongs to a hexagonal, non-centrosymmetric space group, this material should manifest a nonzero second-order NLO efficiency. The Fig. 5 presents the dependences of the second harmonic intensity generated in the ZnO films, undoped and Ag-, Cu-doped, as the function of incident angle.

As it is usual for *c*-oriented ZnO films, one can observe *M*-shape angular dependence with a maximum signal for 40–55° and zero intensity at normal incidence of the fundamental beam due to the lack of noncentrosymmetry in this direction. The polarization of the second harmonic signal was found to be always *p*-polarized regardless of the incident polarization. The observed angular dependences are related to the crystalline symmetry when there is preferred axis orientation that is in (0 0 2) direction [32–34].

Fig. 6 presents the second harmonic signal from the ZnO films, undoped and doped by Ag and Cu with different concentration, plotted vs. the square of incident intensity. These data demonstrate the quadratic power law, expected for SHG. At the fundamental intensity of 4 GW/cm^2 the conversion efficiencies to the second harmonic were calculated and their specific values (as the samples have different thickness) are presented in Table 2. As it is evident from Fig. 6 and Table 2, the undoped ZnO film exhibits higher second-order NLO response than the doped film. The specific SHG conversion efficiency of Ag- and Cu-doped ZnO films is one–two orders of magnitude lower than those in the undoped ZnO. Moreover, the conversion efficiency in second harmonic for

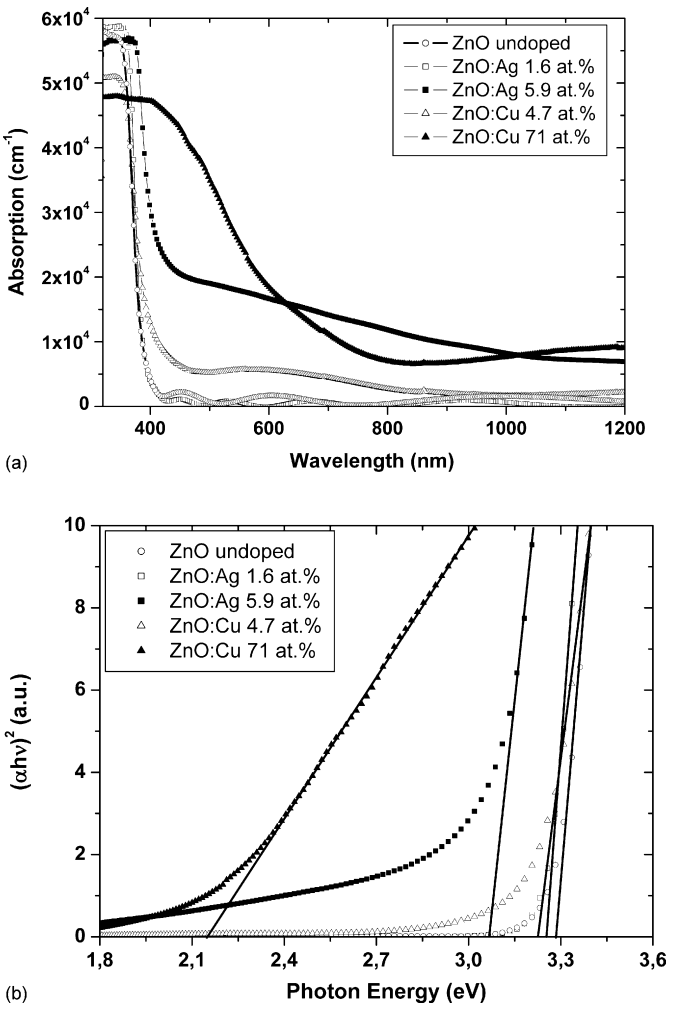

Fig. 4. (a) Room-temperature UV-visible absorption spectra of the ZnO films, undoped and doped by Ag, Cu, (b) the dependence $(\alpha h\nu)^2$ vs. photon energy ($h\nu$). Solid lines correspond to extrapolation fit.

p–p geometry of experiment is one order higher than for s–p configuration.

Besides, the ZnO films doped by Ag and Cu at the similar concentration (5.9 and 4.7 at.%) demonstrate different efficiency of SHG. The main reason consists in the differences of crystalline structure of ZnO after incorporation of dopant. The copper ions incorporated into ZnO matrix distort the lattice more than the ions of silver due to their smaller radius, meanwhile, the ions of silver either substitute zinc ions or aggregate within ZnO boundaries.

Moreover, one can see that with increasing of Ag dopant from 1.6 to 5.9 at.% a small increment of the second-order NLO response is observed. Such a behaviour can be explained by modified polycrystalline structure of ZnO film caused by increased concentration of Ag dopant. In the ZnO film doped by Cu with high concentration of 71 at.%, e.g., when most Zn atoms are substituted by Cu atoms the crystalline structure of film suffers a loss of noncentrosymmetry or even become amorphous.

Table 2
Specific SHG conversion efficiency in Ag- and Cu-doped ZnO films.

Film	η/d (cm^{-1}) (s–p)	η/d (cm^{-1}) (p–p)
ZnO undoped	1.9×10^{-3}	1.5×10^{-2}
ZnO:Ag (1.6 at.%)	1.4×10^{-4}	1.9×10^{-3}
ZnO:Ag (5.9 at.%)	1.7×10^{-4}	3.1×10^{-3}
ZnO:Cu (4.7 at.%)	6.5×10^{-5}	1.8×10^{-3}
ZnO:Cu (71 at.%)	6.0×10^{-7}	1.8×10^{-5}

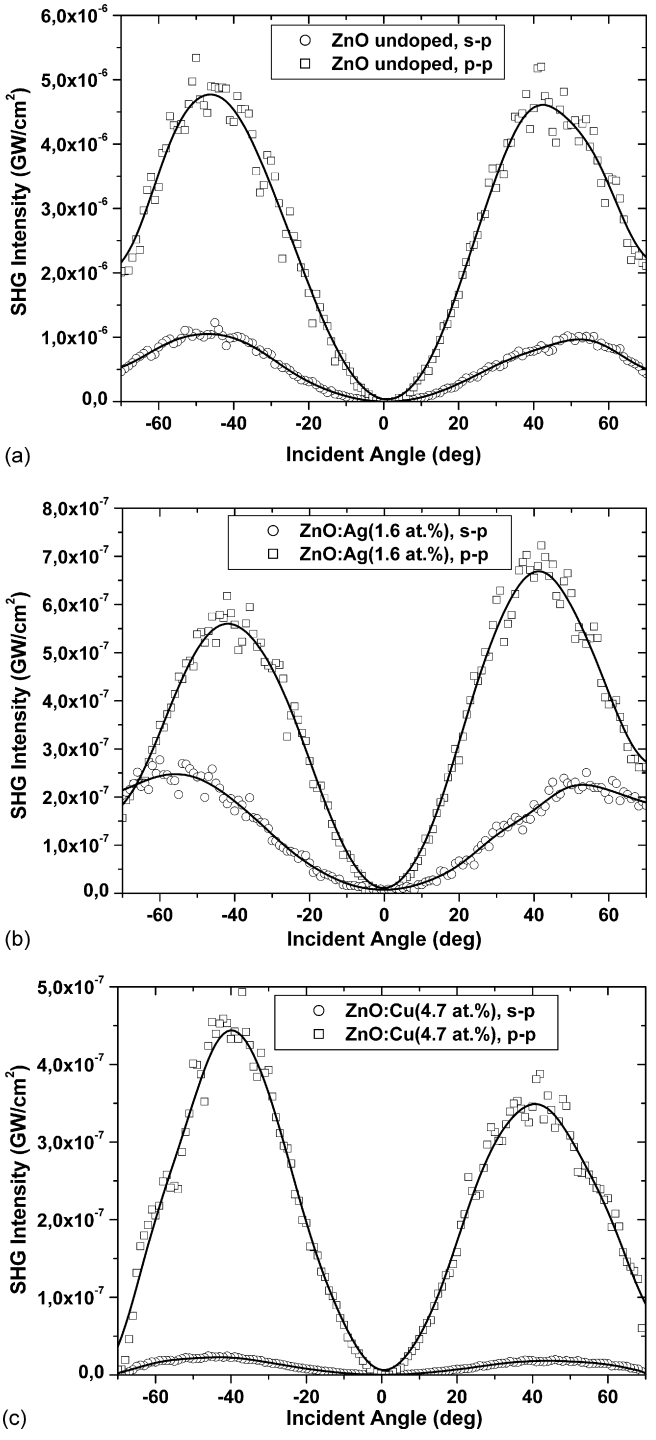

Fig. 5. Second harmonic intensity from (a) ZnO, (b) ZnO:Ag (1.6 at.%) and (c) ZnO:Cu (4.7 at.%) films as a function of incident angle. The fundamental beam is s-, p-polarized and generated is *p*-polarized. Solid curves correspond to fitting.

For an isotropic, absorbing nonlinear material, deposited on the substrate, neglecting reflections, we have the following expression for transmitted second harmonic intensity [29]:

$$I_{2\omega}^{s\to p}(\theta) = \frac{128\pi^5}{c\lambda^2}\frac{[t_{af}^{1s}]^4[t_{fs}^{2p}]^2[t_{sa}^{2p}]^2}{n_{2\omega}^2\cos^2\theta_{2\omega}} I_\omega^2 (L\chi_{\text{eff}}^{(2)})^2 \exp[-2(\delta_1+\delta_2)]\frac{\sin^2\Phi+\sinh^2\Psi}{\Phi^2+\Psi^2}, \quad (3)$$

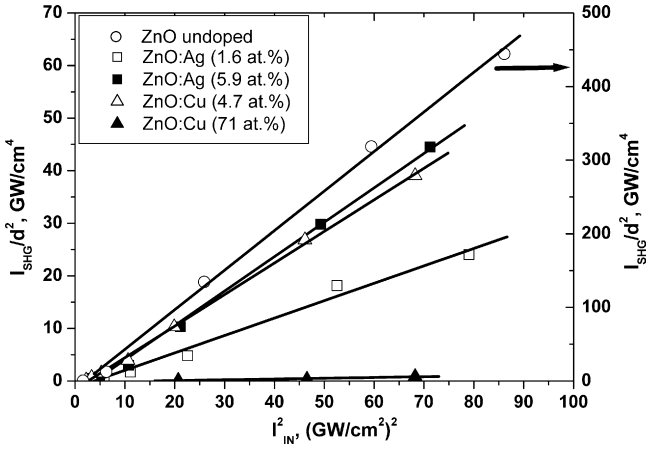

Fig. 6. Dependence of the SHG intensity per square of films thickness vs. square of intensity of s-polarized incident beam for undoped and Ag-, Cu-doped ZnO films. Solid curves correspond to linear fitting.

where I_ω – intensity of the pump wave, λ – wavelength of pump wave, $\chi^{(2)}_{\text{eff}}$ – the effective second-order nonlinear susceptibility, n_ω, $n_{2\omega}$ – the refractive indices for the pump and harmonic waves, L – the film thickness, t_{af}^{1s}, t_{fs}^{2p}, t_{sa}^{2p} – the Fresnel transmission coefficients (air–film–substrate–air system) for fundamental and SHG beam. The phase angle Φ and Ψ can be expressed [29]:

$$\Phi = \frac{2\pi L}{\lambda}(n_\omega\cos\theta_\omega - n_{2\omega}\cos\theta_{2\omega}), \quad (4)$$

$$\Psi = \delta_1 - \delta_2 = \frac{2\pi L}{\lambda}\left(\frac{n_\omega\kappa_\omega}{\cos\theta_\omega} - \frac{n_{2\omega}\kappa_{2\omega}}{\cos\theta_{2\omega}}\right), \quad (5)$$

where θ_ω, $\theta_{2\omega}$ – the fundamental and generated beams refractive angles determined by the law of diffraction, κ_ω, $\kappa_{2\omega}$ – the extinction coefficients of the nonlinear material at frequencies ω and 2ω.

$\chi^{(2)}_{\text{eff}}$ in Eq. (3) represents the effective second-order susceptibility. Since ZnO has hexagonal close packed structure, with the 6 mm symmetry, individual crystallite should have only four independent nonzero components of the second-order susceptibility tensor [32]: $\chi^{(2)}_{xzx} = \chi^{(2)}_{yzy}$, $\chi^{(2)}_{xxz} = \chi^{(2)}_{yyz}$, $\chi^{(2)}_{zxx} = \chi^{(2)}_{zyy}$ and $\chi^{(2)}_{zzz}$, where the coordinates correspond to the crystal axes of individual crystallite. When the frequencies involved are far from resonances, Kleinman's symmetry condition can be applied to further reduce the number of independent components to two: $\chi^{(2)}_{xzx} = \chi^{(2)}_{yzy} = \chi^{(2)}_{xxz} = \chi^{(2)}_{yyz} = \chi^{(2)}_{zxx} = \chi^{(2)}_{zyy}$ and $\chi^{(2)}_{zzz}$. Because the tensorial property of the ZnO film is equivalent to that of an isotropic uniaxial medium, the experimental observation of the SHG signal is always *p*-polarized no matter the fundamental beam is s- or p-polarized [32].

Therefore, when the fundamental beam is s-polarized,

$$\chi^{(2)}_{\text{eff}} = \chi^{(2)}_{zxx}\sin\theta_{2\omega}. \quad (6)$$

When the fundamental beam is p-polarized,

$$\chi^{(2)}_{\text{eff}} = \chi^{(2)}_{zxx}(\cos\theta_{2\omega}\sin 2\theta_\omega + \sin\theta_{2\omega}\cos^2\theta_\omega) + \chi^{(2)}_{zzz}\sin\theta_{2\omega}\sin^2\theta_\omega. \quad (7)$$

To estimate the absolute values of the second-order nonlinear susceptibility tensor components of the Ag-, Cu-doped ZnO films we used the expression for SHG Eq. (1) together with Eqs. (6) and (7). The results are presented in Table 3. As one might expect the ZnO films, doped by Ag or Cu, are characterized by lower value of $\chi^{(2)}_{zxx}$ in comparison with undoped ZnO film. And in the case of Cu doping this decrease of $\chi^{(2)}$ is more noticeable due to the difference in sizes of Ag and Cu ions incorporated into ZnO lattice. Although the highest value of $\chi^{(2)}_{zzz}$ are obtained for the ZnO film doped by Cu with 4.7 at.%.

Table 3
Second-order NLO susceptibility tensor components for undoped and Ag-, Cu-doped ZnO films.

Film	$\chi^{(2)}_{zxx}$ (pm/V)	$\chi^{(2)}_{zzz}$ (pm/V)
ZnO pure	4.6	7.0
ZnO:Ag(1.6 at.%)	1.0	14
ZnO:Ag(5.9 at.%)	1.5	13
ZnO:Cu(4.7 at.%)	1.4	17
ZnO:Cu(71 at.%)	0.2	2.0
ZnO bulk [31]	3.5	−12

Table 4
Effective values of third-order NLO susceptibility for undoped and Ag-, Cu-doped ZnO films.

Film	$\chi^{(3)}_{eff}$ (10^{-20} m^2/V^2)
ZnO undoped	5.7
ZnO:Ag(1.6 at.%)	2.1
ZnO:Ag(5.9 at.%)	1.2
ZnO:Cu(4.7 at.%)	3.5
ZnO:Cu(71 at.%)	1.9
ZnO bulk [36]	0.17

3.4. THG measurements

The third-order optical nonlinearities of Ag-, Cu-doped ZnO films were investigated by THG technique in order to study the effect of doping on the cubic nonlinear response.

The THG angle dependences collected in Fig. 7 originate from the ZnO films together with substrates, since the THG process can occur in any material regardless of its symmetry. However, the effect of glass substrate in THG process is comparatively diminutive and negligible as compared with ZnO film. Fig. 7 illustrates the series of the THG angle dependences of the doped ZnO films with different concentrations of dopant. The highest THG intensity is obtained in the undoped ZnO film, which is slightly higher than in Ag-, Cu-doped ZnO films. It is interesting to note that Cu-doped ZnO film demonstrates higher THG efficiency than Ag-doped at the similar concentration of dopant. The differences in embedding of Ag and Cu ions into ZnO can explain this fact. Ag ions incorporated into ZnO due to their larger radius mostly substitute Zn ions in their places, and in the charge state Ag^+, the ZnO lattice has a lack of electrons, e.g., its resistance increase [19]. Meanwhile, ions of Cu incorporated into ZnO even at low concentrations can occupy both lattice and interstitial sites, thus, increasing concentration of electrons in ZnO. As it is known, the peculiarities of the crystalline structure do not play so considerable role in THG process as presence of the charge carriers. Therefore, the THG efficiency of Cu-doped ZnO film is higher than that of Ag-doped one. Moreover, ZnO film doped by Cu with 71 at.% manifests a quite high third-order NLO response. This confirms that THG process is not such dependent on crystalline structure of medium as SHG process.

According to the work of Wang et al. [35] the intensity of the THGs in a nonlinear film upon a substrate in air ambient is given by

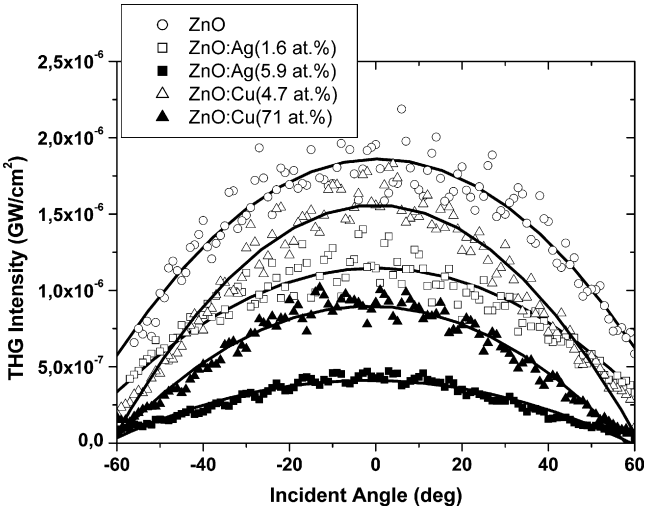

Fig. 7. The THG experimental results for the ZnO film and Ag-, Cu-doped ZnO films. The fundamental beam is s-polarized and laser intensity is about 15 GW/cm^2. Solid curves correspond to fitting.

the following expression:

$$I^{3\omega} = \frac{64\pi^4}{c^2}\left|\frac{\chi_s^{(3)}}{\Delta\varepsilon_s}\right|(I^{\omega})^3 |e^{i(\psi_s^{3\omega}+\psi_f^{\omega})}[T_1(e^{i\Delta\psi_s}-1) + \rho e^{i\phi}T_2(1-e^{-i\Delta\psi_f})] + C_{air}|^2, \quad (8)$$

where

$$\rho e^{i\phi} = \frac{|\chi_f^{(3)}/\Delta\varepsilon_f|}{|\chi_s^{(3)}/\Delta\varepsilon_s|}, \quad (9)$$

$\chi^{(3)}{}_f$, $\chi^{(3)}{}_s$ – the third-order effective nonlinear susceptibility of the film and substrate, $\Delta\varepsilon_f$, $\Delta\varepsilon_s$ – the dispersion of the dielectric constants, C_{air} – the contribution of air, $\Delta\Psi_s$, $\Delta\Psi_f$ – the phase angles in substrate and film, respectively. The detailed description of calculation of the cubic nonlinear susceptibilities could be found in [11].

Using the Eq. (8), we calculated the effective values of the cubic nonlinear susceptibilities for the undoped and doped ZnO films (Table 4). The maximal value was obtained for the undoped ZnO film: $\chi^{(3)}{}_{eff} = 5.65 \times 10^{-20}$ m^2/V^2. This value is one order of magnitude higher than that of ZnO bulk crystal and is in good correlation with those already reported for ZnO films [28,36,37]. It also should be noted that even for input intensities in the range of 15 GW/cm^2 no structural change or damage of the objects occurred.

4. Conclusions

Ag- and Cu-doped ZnO films with various Ag, Cu contents were prepared by RF-magnetron sputtering on glass and quartz substrates. The structural, morphological and optical properties of the deposited films were found to be dependent on the dopant content. The optical gap narrowing was observed for all doped ZnO films due to the substitution of zinc ions by Ag or Cu ions. Besides, the second-order NLO response of Ag- and Cu-doped ZnO films was obtained to be lower than that of the undoped ZnO film. Likewise, THG response of undoped ZnO films is higher than that of doped ones. Therefore, we can conclude that SHG as well as THG processes in ZnO films are strongly dependent on the dopant type and its amount. At the same time, one can conclude that the doped ZnO films should be considered as the attractive materials for the photoinduced NLO effects. The corresponding phenomena such as photoinduced SHG are expected to be investigated carefully for its potential application in the nearest future.

Acknowledgments

The authors acknowledge the Service Commun d'Imageries et Analyses Microscopiques of University of Angers for performing AFM measurements. The authors thank R. Serkiz of Scientific-Technical and Educational Center of Low Temperature Studies of Lviv for performing SEM and EDX measurements. This work is also supported by INTAS (ref. no. 06-1000019-6137) and Ministry of Science and Education of Ukraine.

References

[1] B.J. Lokhande, M.D. Uplane, Appl. Surf. Sci. 167 (2000) 243–246.
[2] R. Triboulet, J. Perrière, Prog. Cryst. Growth Charact. Mater. 47 (2003) 65–138.
[3] E. Fortunato, P. Barquinha, A. Pimentel, L. Pereira, A. Gonçalves, A. Marques, R. Martins, L. Pereira, Appl. Phys. Lett. 85 (2004) 2541.
[4] D. Brida, E. Fortunato, I. Ferreira, H. Aguas, R. Martins, J. Non-Cryst. Solids 299–302 (2002) 1272–1276.
[5] Ü. Özgür, Ya.I. Alivov, C. Liu, A. Teke, M.A. Reshchikov, S. Doğan, V. Avrutin, S.-J. Cho, H. Morkoç, J. Appl. Phys. 98 (2005) 1–103.
[6] S.H. Jeong, B.N. Park, S.B. Lee, J.-H. Boo, Surf. Coat. Technol. 193 (2005) 340–344.
[7] L. Duan, W. Gao, R. Chen, Z. Fu, Solid State Commun. 145 (2008) 479–481.
[8] X.B. Wang, D.M. Li, F. Zeng, F. Pan, J. Phys. D: Appl. Phys. 38 (2005) 4104–4108.
[9] S.H. Jeong, D.G. Yoo, D.Y. Kim, N.E. Lee, J.H. Boo, Thin Solid Films 516 (19) (2008) 6598–6603.
[10] X. Peng, J. Xu, H. Zang, B. Wang, Z. Wang, J. Lumin. 128 (2008) 297–300.
[11] B. Kulyk, Z. Essaidi, J. Luc, Z. Sofiani, G. Boudebs, B. Sahraoui, V. Kapustianyk, B. Turko, J. Appl. Phys. 102 (1–6) (2007) 113113.
[12] T. Kryshtab, V.S. Khomchenko, V.B. Khachatryan, N.N. Roshchina, J.A. Andraca-Adame, O.S. Lytvyn, V.I. Kushnirenko, J. Mater. Sci. Mater. Electron 18 (2007) 1115–1118.
[13] V.S. Khomchenko, T.G. Kryshtab, A.K. Savin, L.V. Zavyalova, N.N. Roshchina, V.E. Rodionov, O.S. Lytvyn, V.I. Kushnirenko, V.B. Khachatryan, J.A. Andraca-Adame, Superlattices Microstruct. 42 (2007) 94–98.
[14] M. Öztas, M. Bedir, Thin Solid Films 516 (2008) 1703–1709.
[15] R. Deng, Y. Zou, H. Tang, Physica B 403 (2008) 2004–2007.
[16] A. Tiwari, M. Snure, D. Kumar, J.T. Abiade, Appl. Phys. Lett. 92 (2008) 062509.
[17] D. Chakraborti, G.R. Trichy, J.T. Prater, J. Narayan, J. Phys. D: Appl. Phys. 40 (2007) 7606–7613.
[18] S.W. Xue, X.T. Zu, W.L. Zhou, H.X. Deng, X. Xiang, L. Zhang, H. Deng, J. Alloys Compd. 448 (2008) 21–26.
[19] S.T. Kuo, W.H. Tuan, J. Shieh, S.F. Wang, J. Eur. Ceram. Soc. 27 (2007) 4521–4527.
[20] Y. Zhang, L. Wu, H. Li, J. Xu, L. Han, B. Wang, Z. Tuo, E. Xie, J. Alloys Compd. 473 (2009) 319–322.
[21] P. Singh, A. Kaushal, D. Kaur, J. Alloys Compd. 471 (2009) 11–15.
[22] T. Ratana, P. Amornpitoksuk, T. Ratana, S. Suwanboon, J. Alloys Compd. 470 (2009) 408–412.
[23] A.N. Gruzincev, V.T. Volkov, E.E. Yakimov, Phys. Tech. Semicond. 37 (2003) 275–278.
[24] I.V. Kityk, J. Ebothé, I. Fuks-Janczarek, A. Ali Umar, K. Kobayashi, M. Oyama, B. Sahraoui, Nanotechnology 16 (2005) 1687–1692.
[25] J.C. Johnson, H. Yan, R.D. Schaller, P.B. Petersen, P. Yang, R.J. Saykally, NanoLetters 2 (2002) 279–283.
[26] M. Alaoui Lamrani, M. Addou, Z. Sofiani, B. Sahraoui, J. Ebothe, A. El Hichou, N. Fellahi, J.C. Bernede, R. Dounia, Opt. Commun. 277 (1) (2007) 196–201.
[27] B. Kulyk, Z. Essaidi, V. Kapustianyk, B. Turko, V. Rudyk, M. Partyka, M. Addou, B. Sahraoui, Opt. Commun. 281 (2008) 6107–6111.
[28] Z. Sofiani, B. Sahraoui, M. Addou, R. Adhiri, M.A. Lamrani, L. Dghoughi, N. Fellahi, B. Derkowska, W. Bala, J. Appl. Phys. 101 (1–5) (2007) 063104.
[29] W.N. Herman, L.M. Hayden, J. Opt. Soc. Am. B 12 (1995) 416–427.
[30] Q. Wan, Z. Xiong, J. Dai, J. Rao, F. Jiang, Opt. Mater. 30 (2008) 817–821.
[31] M.J. Weber, Handbook of Optical Materials, CRC Press, Boca Raton, FL, 2003.
[32] H. Cao, J.Y. Wu, H.C. Ong, J.Y. Dai, R.P.H. Chang, Appl. Phys. Lett. 73 (1998) 572–574.
[33] C.Y. Liu, B.P. Zhang, N.T. Binh, Y. Segawa, Opt. Commun. 237 (2004) 65–70.
[34] M.C. Larciprete, D. Haertle, A. Belardini, M. Bertolotti, F. Sarto, P. Gunter, Appl. Phys. B: Lasers Opt. 82 (2006) 431–437.
[35] X.H. Wang, D.P. West, N.B. McKeown, T.A. King, J. Opt. Soc. Am. B 15 (1998) 1895–1903.
[36] C.Y. Liu, B.P. Zhang, N.T. Binh, Y. Segawa, Appl. Phys. B: Lasers Opt. 79 (2004) 83–86.
[37] G.I. Petrov, V. Shcheslavskiy, V.V. Yakovlev, I. Ozerov, E. Chelnokov, W. Marine, Appl. Phys. Lett. 83 (2003) 3993–3995.